Available online at www.sciencedirect.com
SCIENCE DIRECT®
ELSEVIER
Nuclear Instruments and Methods in Physics Research B 235 (2005) 438–442
NIM B
Beam Interactions with Materials & Atoms
www.elsevier.com/locate/nimb

Energy- and angular-distributions of F^+ ions emitted from a F-terminated Si(100) surface with slow highly charged ions

N. Okabayashi [a,*], K. Komaki [a], Y. Yamazaki [a,b]

[a] *Institute of Physics, Graduate School of Arts and Sciences, University of Tokyo, 3-8-1 Komaba, Meguro, Tokyo 153-8902, Japan*
[b] *Atomic Physics Laboratory, RIKEN, 2-1 Hirosawa, Wako, Saitama 351-0198, Japan*

Available online 11 May 2005

Abstract

Time and two-dimensional position distributions of F^+ ions emitted from a well-defined F/Si(100)-2×1 target were measured for impact of slow highly charged ions of 3.9 keV Ar^{5+}. The time and position distributions were transformed into energy and angular distributions, which revealed that the peak emission energy was 2.0 ± 0.6 eV and the emission angle measured from the surface normal was $18 \pm 4°$ in the (011) or $(01\bar{1})$ plane.

PACS: 79.20.La; 79.20.Rf

Keywords: Fluorine; Si(100); Highly charged ions; Potential sputtering

1. Introduction

Secondary particle emissions induced with slow highly charged ion (HCI) impact have been intensively studied for the last two decades to understand basic atomic processes involved in sputtering phenomena and to apply the phenomena for various fields of sciences [1,2]. Because an HCI has large potential energy and strong electric field, it can induce emission of secondary particles via electronic transitions (potential sputtering) [3–7] as well as via recoil momentum transfer (kinetic sputtering).

In order to elucidate the mechanism of potential sputtering, measurements of emission angle and emission energy are expected to provide key information on the involved processes. It was not easy and straightforward to extract such information because of contaminant secondary ions induced by momentum transfer from the incident ions (kinetic sputtering). Recently, we constructed an

* Corresponding author. Present address: Institute of Multidisciplinary Research for Advanced Materials, Tohoku University, Katahira 2-1-1, Sendai, 980-8577, Japan. Tel.: +81 22 217 5369; fax: +81 22 217 5371.
E-mail address: norio@radphys4.c.u-tokyo.ac.jp (N. Okabayashi).

0168-583X/$ - see front matter
doi:10.1016/j.nimb.2005.03.220

experimental setup with a two-dimensional position sensitive detector (2D-PSD) having good time resolution (≈ns) [6], by which mass resolved angular- and energy-distributions could be obtained.

In the present paper, we report the first result of the energy- and angular-distributions of F^+ ions emitted from a well-defined F/Si(1 0 0)-2 × 1 surface bombarded with 3.9 keV Ar^{5+} ions. The transform scheme and analysis procedures are discussed in detail.

2. Experimental setup and data analysis

Fig. 1 shows a schematic drawing of the secondary ion detection system. HCIs were extracted from a mini-EBIS [8], charge-state selected with a Wien-filter, periodically swept with a deflector to form a 50 kHz pulse train, 50 ns wide, and guided into a target chamber. When a pulsed HCI beam impacts on the surface, some constituents of the target are emitted as secondary particles. Positively charged secondary ions are accelerated normal to the surface by the electric field applied between the target and the grounded mesh (the spacing is l_1). After the mesh, secondary ions travel in the field free region (the length is l_2) and finally impinge on the two-dimensional position sensitive detector (2D-PSD). The 2D-PSD provides information on 2D-position (X and Y) and time of flight (TOF, t) of each secondary ion. The position and time signals are digitized and accumulated as a three-dimensional distribution, $n(X, Y, t)$.

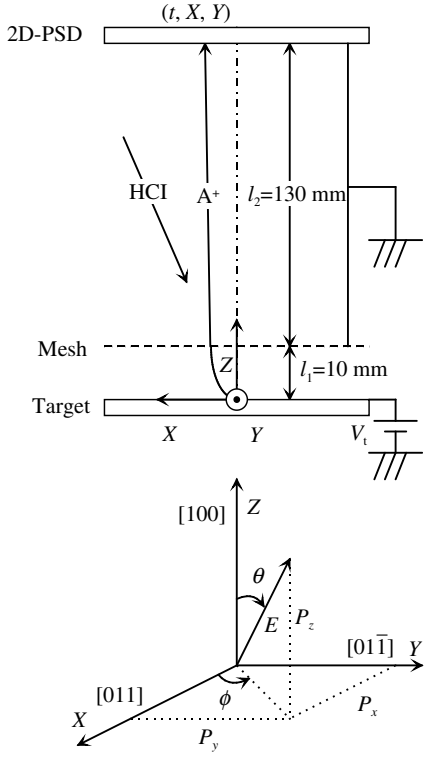

Fig. 1. Schematic drawing of the secondary ion detection system.

Three components of the momentum, (P_x, P_y, P_z), and the energy, polar angle and azimuthal angle, (E, θ, ϕ), of the emitted ion are calculated from (X, Y, t). The TOF is given by

$$t = \sqrt{2m}\left(\frac{\sqrt{qV_t + P_z^2/2m} - \sqrt{P_z^2/2m}}{qV_t} l_1 + \frac{1}{2\sqrt{qV_t + P_z^2/2m}} l_2\right), \quad (1)$$

as a function of the longitudinal momentum P_z, where V_t is the target bias, m and q are the mass and charge of secondary ion, respectively. The lateral momenta, P_x and P_y, are given by

$$P_x = mX/t, \quad P_y = mY/t. \quad (2)$$

The 3D-momenta are converted to the energy E, polar angle θ and azimuthal angle ϕ by

$$E = \left(P_x^2 + P_y^2 + P_z^2\right)\Big/2m, \quad \theta = \arctan\left(P_z\Big/\sqrt{P_x^2 + P_y^2}\right), \quad \phi = \arctan(P_y/P_x). \quad (3)$$

Employing Eqs. (1)–(3), $n(X, Y, t)$ can be converted to $h(E, \theta, \phi; m)$ for the specified ion mass, m, by

$$n(X, Y, t) \cdot \mathrm{d}t \cdot \mathrm{d}X \cdot \mathrm{d}Y = h(E, \theta, \phi; m) \cdot \sin\theta \cdot \mathrm{d}\theta \cdot \mathrm{d}\phi \cdot \mathrm{d}E. \quad (4)$$

The 2D-positional distribution in the TOF range from t_i to t_f, $f(X, Y; t_i, t_f)$, and the TOF distribution, $g(t)$, are derived from the $n(X, Y, t)$ using

$$f(X,Y;\,t_{\rm i},t_{\rm f}) = \int_{t_{\rm i}}^{t_{\rm f}} n(X,Y,t)\cdot {\rm d}t,$$
$$g(t) = \iint n(X,Y,t)\cdot {\rm d}X\cdot {\rm d}Y. \tag{5}$$

The energy distribution, $p(E)$, and the angular distribution, $r(\theta,\phi)$, are derived from the $h(E,\theta,\phi;m)$ using

$$p(E) = \iint h(E,\theta,\phi;m)\cdot\sin\theta\cdot {\rm d}\theta\cdot {\rm d}\phi,$$
$$r(\theta,\phi) = \int h(E,\theta,\phi;m)\cdot {\rm d}E. \tag{6}$$

Errors transferred to the 3D-momenta from those in the TOF, Δt, and in the positions, ΔX and ΔY, are given by

$$\Delta P_z = \sqrt{\frac{8qm}{P_z^2}}\left(\left(\frac{2}{\sqrt{V_{\rm t}+E_z}}-\frac{2}{\sqrt{E_z}}\right)\frac{l_1}{V_{\rm t}} - \frac{1}{(V_{\rm t}+E_z)^{2/3}}l_2\right)^{-1}\Delta t,$$
$$\Delta P_x = \sqrt{(P_x\cdot\Delta X/X)^2+(P_x\cdot\Delta t/t)^2},$$
$$\Delta P_y = \sqrt{(P_y\cdot\Delta Y/Y)^2+(P_y\cdot\Delta t/t)^2}, \tag{7}$$

where $E_z = P_z^2/2m$, and errors transferred to energy, ΔE, and polar angle, $\Delta\theta$, are given by

$$\Delta E = \sqrt{(P_x\cdot\Delta P_x)^2+(P_y\cdot\Delta P_y)^2+(P_z\cdot\Delta P_z)^2}/m,$$
$$\Delta\theta = \sqrt{\left(\frac{1}{1+(P_r/P_z)^2}\frac{P_x\cdot\Delta P_x+P_y\cdot\Delta P_y}{P_r\cdot P_z}\right)^2+\left(\frac{1}{1+(P_r/P_z)^2}\frac{P_r\cdot\Delta P_z}{P_z^2}\right)^2}, \tag{8}$$

where $P_r = \sqrt{P_x^2+P_y^2}$.

3. Results and discussion

A three-dimensional distribution, $n(X,Y,t)$, which consists of $\approx 10^6$ events, was accumulated for F^+ and Si^+ emitted from the F/Si(1 0 0)-2 × 1 surface irradiated by 3.9 keV Ar^{5+} ions incident at 30° with respect to the surface normal. Fig. 2(a) shows an example of the TOF spectrum, where the time range is selected for F^+ and Si^+ ions. It is seen that the Si^+ peak, skewing to shorter flight time, is distributed over more than 2 μs. On the other hand, the F^+ peak at 3.9 μs extends from t_2 to t_3 ($\tau = t_3 - t_2 \approx 0.2$ μs). Considering the pulse width of the HCI beam is 50 ns, the intrinsic TOF distribution of F^+ ions is estimated to be 90 ns full width at half maximum. Fig. 2(b) shows $f(X,Y;t_2,t_3)$, the 2D-positional distribution of ions in the TOF range from t_2 to t_3 depicted in Fig. 2(a). As is seen in Fig. 2(a), $f(X,Y;t_2,t_3)$ consists not only of F^+ ions but also of Si^+ ions, i.e.

$$f(X,Y;t_2,t_3) = f_{\rm F}(X,Y;t_2,t_3) + f_{\rm Si}(X,Y;t_2,t_3). \tag{9}$$

In order to evaluate $f_{\rm Si}(X,Y;t_2,t_3)$, we assume

$$f_{\rm Si}(X,Y;t_2,t_3) \approx f(X,Y;t_1,t_2)/2 + f(X,Y;t_3,t_4)/2, \tag{10}$$

where $t_2 - t_1 = t_4 - t_3 = \tau$. Fig. 2(c) and (d) shows $f(X,Y;t_1,t_2)$ and $f(X,Y;t_3,t_4)$, respectively, and Fig. 2(e) shows resultant $f_{\rm F}(X,Y;t_2,t_3)$, i.e.

$$f_{\rm F}(X,Y;t_2,t_3) \approx f(X,Y;t_2,t_3) - f(X,Y;t_1,t_2)/2 - f(X,Y;t_3,t_4)/2. \tag{11}$$

As is seen, the four-peak structure indicated in Fig. 2(b) shows up clearly in Fig. 2(e) with each peak at 7 mm from the center along the crystallographic directions of the Si(1 0 0) surface, i.e. [0 1 1] and $[01\bar{1}]$, which corresponds to the direction of F–Si bond on Si(1 0 0) surface [9]. Considering that the spot size of the incoming HCI is 2 mm in diameter, the intrinsic distribution width of the F^+ ions is estimated to be 9 mm full width at half maximum.

The (E,θ,ϕ) distribution of ions detected in the TOF range from $t_{\rm i}$ to $t_{\rm f}$, assuming the mass is m, is denoted as $h(E,\theta,\phi;t_{\rm i},t_{\rm f},m)$. The calculated (E,θ,ϕ) distribution for the blue colored area in Fig. 2(a) is decomposed into two components originating from F^+ and Si^+, as follows:

$$h(E,\theta,\phi;t_2,t_3,19) = h_{\rm F}(E,\theta,\phi;t_2,t_3,19) + h_{\rm Si}(E,\theta,\phi;t_2,t_3,19). \tag{12}$$

The $h_{\rm Si}(E,\theta,\phi;t_2,t_3,19)$ was evaluated by

$$h_{\rm Si}(E,\theta,\phi;t_2,t_3,19) \approx h'(E,\theta,\phi;t_1,t_2,19)/2 + h''(E,\theta,\phi;t_3,t_4,19)/2, \tag{13}$$

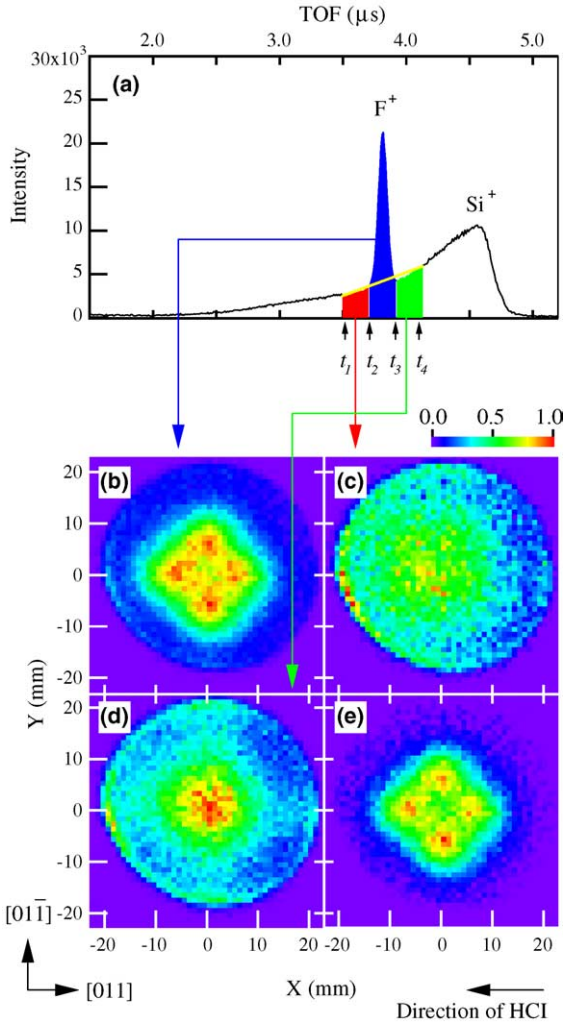

Fig. 2. (a) An example of TOF spectrum of F^+ and Si^+ emitted from the F/Si(1 0 0)-2 × 1 surface irradiated by 3.9 keV Ar^{5+} ions. (b)–(d) 2D-positional distributions of secondary ions: $f(X, Y; t_2, t_3)$, $f(X, Y; t_1, t_2)$, $f(X, Y; t_3, t_4)$, and $f_F(X, Y; t_2, t_3)$, respectively.

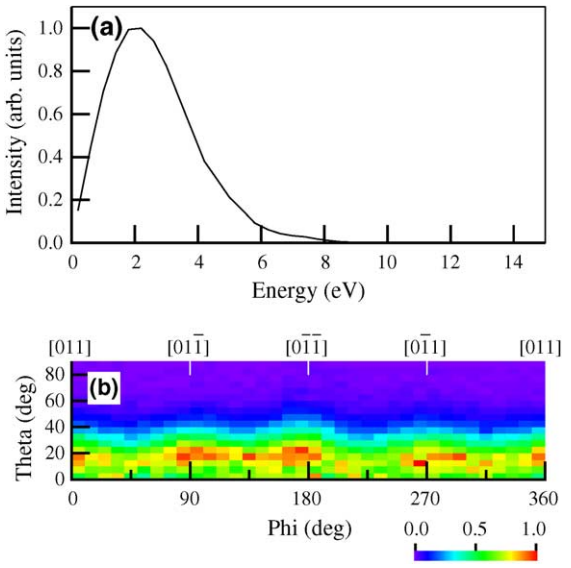

Fig. 3. (a) The energy distribution and (b) the angular distribution of F^+ ions emitted from the F/Si(1 0 0)-2 × 1 surface irradiated by 3.9 keV Ar^{5+} ions.

where $h'(E, \theta, \phi; t_1, t_2, 19)$ and $h''(E, \theta, \phi; t_3, t_4, 19)$ mean that the origin of the times are shifted by $-\tau$ and $+\tau$, respectively, when t is converted into P_z with Eq. (1).

Fig. 3(a) and (b) shows normalized energy- and angular-distributions of F^+ ions, respectively. It is seen that the energy distribution has a peak around 2.0 eV and the polar angle distribution has a peak around 18°. It is noted that the latter value is close to a theoretical prediction, 23° [10].

Most probable values of the energy and polar angle may correspond to most probable 3D momenta: $P_x = 28$ (0) a.u., $P_y = 0$ (28) a.u. and $P_z = 70$ a.u.. Substituting $t = 3.9$ μs, $X(Y) = 7$ mm, $P_z = 70$ a.u., and P_x (P_y) = 28 a.u. into Eq. (7), the 3D-momenta including errors are estimated to be $P_z = 70 \pm 11$ a.u. and P_x (P_y) = 28 ± 2 a.u., respectively, assuming the ambiguity of the time and position are $\Delta t \approx 15$ ns and ΔX (ΔY) ≈ 0.5 mm, respectively. Accordingly, substituting $P_x = 28$ (0) a.u., $P_y = 0$ (28) a.u., $P_z = 70$ a.u., $\Delta P_z = 11$ a.u., and ΔP_x (P_y) = 2 a.u. into Eq. (8), the emission energy and polar angle including errors are estimated to be $E = 2.0 \pm 0.6$ eV and $\theta = 18 \pm 4°$, respectively.

Acknowledgements

We are deeply indebted to K. Ueda, T. Komeda and S. Fukatsu for their various advices, particularly on the sample preparation. Thanks are also

due to K. Kuroki for the discussion on the physical process and advice on the experimental setup.

References

[1] A. Arnau et al., Surf. Sci. 27 (1997) 113.
[2] T. Schenkel, A.V. Hamza, A.V. Barnes, D.H. Schneider, Prog. Surf. Sci. 61 (1999) 23.
[3] N. Kakutani, T. Azuma, Y. Yamazaki, K. Komaki, K. Kuroki, Nucl. Instr. and Meth. B 96 (1995) 541.
[4] J. Burgdörfer, Y. Yamazaki, Phys. Rev. A 54 (1996) 4140.
[5] K. Kuroki, N. Okabayashi, H. Torii, K. Komaki, Y. Yamazaki, Appl. Phys. Lett. 81 (2002) 3561.
[6] N. Okabayashi, K. Komaki, Y. Yamazaki, Nucl. Instr. and Meth. B 205 (2003) 725.
[7] G. Haydere et al., Phys. Rev. Lett. 86 (2001) 3530.
[8] K. Okuno, Jpn. J. Appl. Phys. 28 (1989) 1124.
[9] C. Simpson, J.A. Yarmoff, Surf. Sci. 359 (1996) 135.
[10] C.J. Wu, E.A. Carter, Phys. Rev. B 45 (1992) 9065.